EurJIC European Journal of Inorganic Chemistry

ChemPubSoc Europe

FULL PAPER

DOI:10.1002/ejic.201500507

TeO_2 Nanoparticle Loaded Graphitic Carbon Nitride Hybrids: Their Preparation and Catalytic Activities in the Thermal Decomposition of Ammonium Perchlorate

Qi Li,[a] Yi He,*[b] and Rufang Peng*[a]

Keywords: Hybrid materials / Nanoparticles / Tellurium / Covalent interactions / Thermal decomposition

TeO_2 nanoparticle-loaded graphitic carbon nitride hybrids (TeO_2NPs/g-C_3N_4) were successfully prepared by a calcination strategy. Various characterization and detection techniques were used to analyze its structure and properties. It was found that upon the addition of 10 wt.-% of the as-prepared hybrids, the onset decomposition temperature of ammonium perchlorate (AP) decreased by 104.4 °C. In addition, the addition of TeO_2 NPs resulted in an increase in the surface area up to 8.8 $m^2 g^{-1}$ for g-C_3N_4, which is three times larger than that of the bulk g-C_3N_4 (2.8 $m^2 g^{-1}$). Furthermore, g-C_3N_4 reacted with $HClO_4$ by Lewis acid–base interaction, which resulted in separation of $HClO_4$ from AP lattice. Notably, the separation of the $HClO_4$ gas molecule led to continued decomposition of AP, as this decomposition reaction is reversible. With this in mind, a catalytic mechanism based on Lewis acid–base interaction was proposed to illustrate the catalytic process in the thermal decomposition of AP.

Introduction

Composite solid propellants (CSPs), as the most important power fuel, have a significant effect on the properties of rockets and missiles such as the onset decomposition temperature and burning rates. They are generally composed of a prepolymer (binder), a high energy fuel, and oxidizer salts.[1] Ammonium perchlorate (AP), as a common oxidant, has been widely used in various propellants. The burning behavior of CSPs is strongly dependent on the properties of the thermal decomposition of AP. Both a lower high-temperature decomposition (HTD) temperature and a higher burning rate of AP would lead to a shorter ignition delay time of these propellants.[2] In this regard, to improve the oxidation effects of AP, various catalysts have been explored to catalyze AP so as to decrease its onset decomposition temperature. The most commonly used catalysts are micro/nanometal oxidation, such as CuO,[3] CoO,[4] Co_3O_4,[5] ZnO,[6] NGO,[7] MnO_2,[8] Mn_3O_4,[9] $MgAl_2O_4$,[10] and NiO,[11] as they can decrease the onset decomposition temperature of AP effectively to some extent. However, these existing micro/nanocatalysts suffer from some inevitable disadvantages, such as heavy metal ions, high cost, and complicated preparation process, all of which result in environmental pollution and greatly limit their applications in modern military and industrial fields. Therefore, one way to overcome the disadvantages is to develop novel catalysts for the thermal decomposition of AP that are highly efficient, low costing, and environmentally friendly.

Recently, graphitic carbon nitride (g-C_3N_4) garnered significant concerned because of its characteristics and properties, including its earth abundancy, its low band gap, and its high catalytic activity.[12] In addition, the band gap of g-C_3N_4 is only 2.7 eV.[13] On this basis, g-C_3N_4 has been widely applied in solar water splitting and in the decomposition of AP.[14] Moreover, research aimed at surface modification of g-C_3N_4 has attracted much attention owing to its graphite-like structure. Shalom et al. reported that the SiO_2 nanoparticles (NPs)/g-C_3N_4 composite could be successfully prepared and used in the degradation of organic pollutants (e.g., rhodamine B).[15] There is no doubt that g-C_3N_4-based hybrids would possess a wide application foreground in photocatalysis, sensing, and bioimaging.[16] Notably, the synergetic effect is very important to g-C_3N_4-based hybrids in the field of photocatalysis. Zhang et al. prepared the g-C_3N_4/$ZnFe_2O_4$ hybrid through a one-step solvothermal method, which can effectively degrade methyl orange, improve the electron-transport ability, and increase the lifetime of photoexcited charge carriers.[17] Ye et al. reported the separable Fe_2O_3/g-C_3N_4 photocatalyst, which was used in the degradation of rhodamine B.[18] However, applications of g-C_3N_4-based hybrids as heat catalysts for

[a] School of Materials Science and Engineering, Southwest University of Science and Technology,
1 No.59, Middle Segment of Qinglong Avenue, Pucheng District, Mianyang City, Sichuan Province, P. R. China
E-mail: pengrufang@swust.edu.cn
www.mskl.swust.edu.cn/

[b] School of National Defense Science and Technology, Southwest University of Science and Technology,
1 No. 59, Middle Segment of Qinglong Avenue, Pucheng District, Mianyang City, Sichuan Province, P. R. China
E-mail: yhe2014@126.com

Supporting information for this article is available on the WWW under http://dx.doi.org/10.1002/ejic.201500507.

the thermal decomposition of AP have not yet been reported.

Herein, for the first time we report the preparation of TeO_2NPs/g-C_3N_4 hybrids and discover that they it have a significant catalytic effect on the thermal decomposition of AP. In particular, the hybrids effectively decrease the HTD temperature by 104.4 °C. Furthermore, a catalytic mechanism based on Lewis acid–base interaction is proposed to illustrate the thermal decomposition of AP. Moreover, the addition of TeO_2 NPs not only results in the formation of covalent coordination interactions but also increases the surface area of g-C_3N_4. By means of Lewis acid–base interaction, a molecule of $HClO_4$ separates from the AP lattice, which results in continued decomposition.

Result and Discussion

Characterization of the TeO_2NPs/g-C_3N_4 Hybrids

The synthesis process of the TeO_2NPs/g-C_3N_4 hybrids is shown in Figure S1 (Supporting Information). The structures of the as-prepared hybrids were determined by X-ray diffraction (XRD). As shown in Figure 1 (a), typical XRD peaks of g-C_3N_4 and TeO_2 are observed. All diffraction peaks are in good agreement with the results of previous literature.[12d,13a,19] The parameters of g-C_3N_4 and TeO_2 are consistent with the literature values of JCPDS No. 87-1526 and No. 65-8053, respectively. For TeO_2, the peaks located at 2θ = 26.1, 28.7, 37.3, 48.5, 55.2, and 62.1° correspond to the crystal faces of (110), (111), (200), (212), (114), and (204), respectively. In addition, the peak located at the (101) crystal face is assigned to impurities of Te in the raw material. For g-C_3N_4, the strong XRD peak at 2θ = 27.5° originates from the (002) interlayer diffraction of the graphitic-like structures, and the low-angle diffraction peak at 2θ = 13.3° is derived from in-plane repeating triazine units. Notably, the diffraction peaks of the TeO_2NPs/g-C_3N_4 hybrids located at 2θ = 13.3, 27.5, 37.3, 48.5, 55.2, and 62.1° correspond to the characteristic peaks of TeO_2 and g-C_3N_4. The above results indicate that TeO_2 NPs exist in the as-prepared TeO_2NPs/g-C_3N_4 hybrids.

The XRD results were further confirmed by FTIR spectroscopy. As indicated in Figure 1 (b), the relatively broad band at $\tilde{\nu}$ = 660–680 cm^{-1} is ascribed to the stretching mode of the terminal Te–O bonds of β-TeO_2, and the sharp band at $\tilde{\nu}$ = 760 cm^{-1} is characteristic of the typical stretching mode of the Te–O–Te bonds of α-TeO_2.[20] Moreover, for g-C_3N_4, the bands at $\tilde{\nu}$ = 1246, 1415, and 1636 cm^{-1} are attributed to the typical stretching modes of CN heterocycles, and this demonstrates the formation of an extended network of C–N–C bonds.[12c] The broad bands between $\tilde{\nu}$ = 3000 and 3400 cm^{-1} are ascribed to the secondary and primary amines.[14e] Notably, for the TeO_2NPs/g-C_3N_4 hybrids, the disappearance of bands at $\tilde{\nu}$ = 760 and 680 cm^{-1} for the TeO_2 crystal results because of the fact that melting give rise to the formation of glassy TeO_2.[21] The weak band near $\tilde{\nu}$ = 3300 cm^{-1} replacing the former band at $\tilde{\nu}$ = 3200 cm^{-1} is attributed to a decrease in the absorption of the amino group. The above results indicate that the TeO_2NPs/g-C_3N_4 hybrids were formed during the calcination process.

The morphology of as-prepared g-C_3N_4 and the TeO_2NPs/g-C_3N_4 hybrids was confirmed by field-emission scanning electron microscopy (FESEM). In contrast to the bulk g-C_3N_4 (Figure 2, a), it can be clearly seen that partial

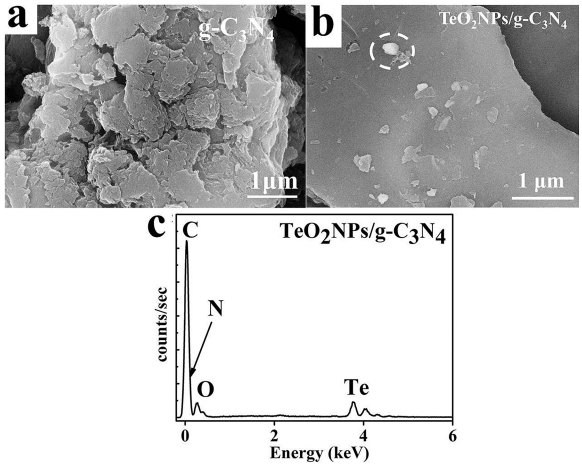

Figure 2. FESEM images of (a) g-C_3N_4 and (b) TeO_2NPs/g-C_3N_4; the white dashed circle emphasizes the TeO_2 NPs. (c) Energy-dispersive X-ray spectrum of the TeO_2NPs/g-C_3N_4 hybrids.

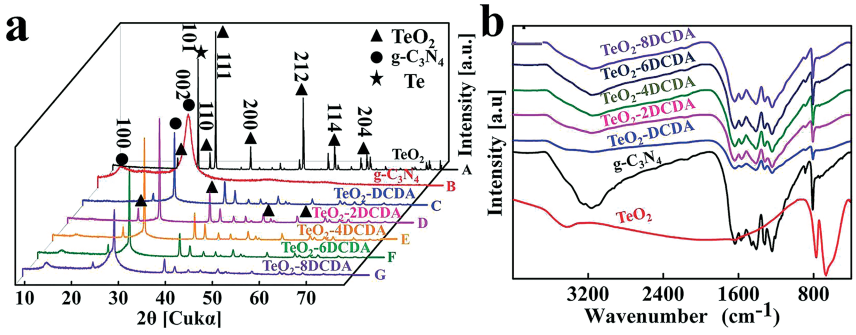

Figure 1. (a) X-ray diffraction patterns and (b) FTIR spectra of the g-C_3N_4-based hybrids prepared from different TeO_2/dicyandiamide (DCDA) weight ratios.

TeO_2 NPs are uniformly dispersed on the surface of a g-C_3N_4 sheet (Figure 2, b). It is easy to understand that the TeO_2 NPs embedded in g-C_3N_4 aggregate during the calcination process of dicyandiamide (DCDA). In addition, Figure 2 (c) shows the energy-dispersive X-ray spectroscopy (EDS) results of the TeO_2NPs/g-C_3N_4 hybrids. Thus, the TeO_2 NPs do exist in the as-prepared sample. Moreover, the enhancement in the thermal catalysis activity of the TeO_2NPs/g-C_3N_4 hybrids is ascribed to the synergistic effects of TeO_2, which lead to an increase in the large surface area of g-C_3N_4 as well as to an improvement in electron transport and efficient separation rate of the electrons and holes.[12d] As indicated in Figure S2, the addition of TeO_2 NPs results in an increase in the surface area up to 8.8 $m^2 g^{-1}$ for g-C_3N_4, which is three times larger than that of the bulk g-C_3N_4 (2.8 $m^2 g^{-1}$).[22]

X-ray photoelectron spectroscopy (XPS) measurements were conducted to further probe the chemical environment and bonding of the C, N, O, and Te atoms in the TeO_2NPs/g-C_3N_4 hybrids. The results suggest that a Te–N covalent interaction[23] is formed between the TeO_2 NPs and the C–NH_x group of g-C_3N_4, which confirms the formation of the TeO_2NPs/g-C_3N_4 hybrids (Figures S3 and S4).

Catalytic Activities of the TeO_2NPs/g-C_3N_4 Hybrids in the Thermal Decomposition of AP

To detect the catalytic activities of the as-prepared hybrids in the thermal decomposition of AP, AP was mixed with g-C_3N_4, TeO_2 NPs, and the TeO_2NPs/g-C_3N_4 hybrids were tested by DSC measurements.

Figure 3a shows the DSC curve of the thermal decomposition of pure AP. The endothermic peak at 245.5 °C is attributed to the crystallographic transition of AP from orthorhombic to cubic.[2a] The exothermic peaks located at 338.9 and 454.4 °C are attributed to low-temperature thermal decomposition (LTD) and the HTD, respectively.[2b,24] Compared to the DSC curve of pure AP, that of AP mixed with TeO_2 NPs (Figure 3, b) exhibits a weak exothermic peak (438.6 °C) because of sublimation of a part of TeO_2.[14e,21a] The DSC curve of AP mixed with g-C_3N_4 is shown in Figure 3 (c); the HTD temperature located at 384.4 °C confirms that g-C_3N_4 possesses an intrinsic catalytic effect on AP.[14d] Notably, the HTD temperature of AP mixed with the TeO_2 NPs and g-C_3N_4 is only 385.7 °C (Figure 3, d), indicating that the independent TeO_2 NPs alone have no acceleration effect. However, the DSC curve

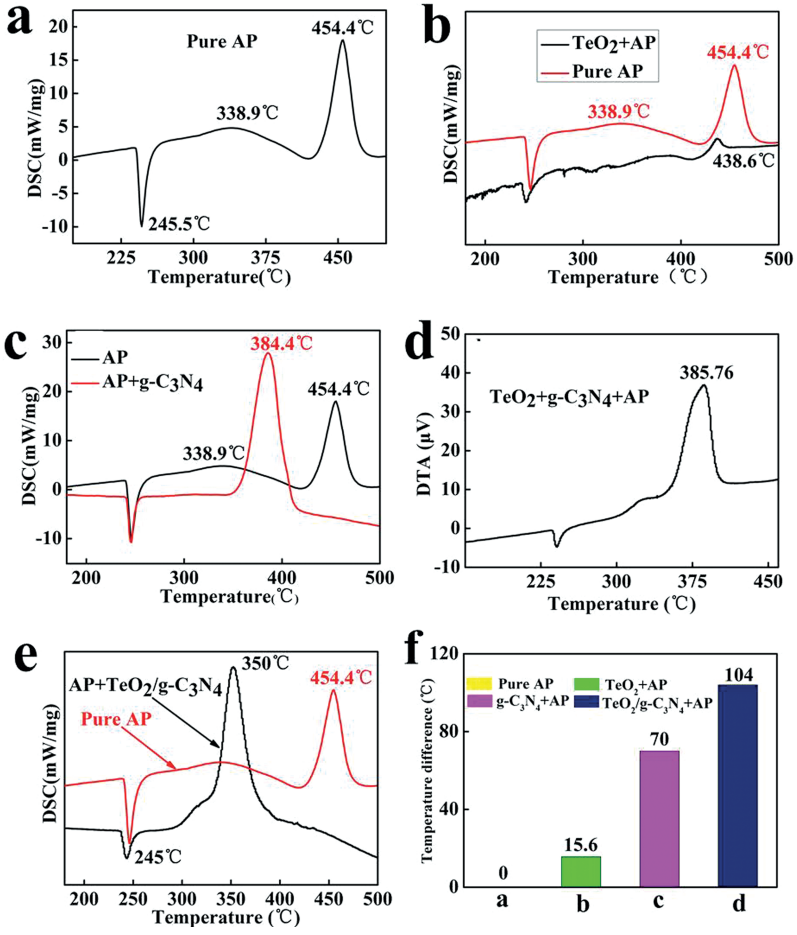

Figure 3. DSC curve of (a) pure AP, (b) AP mixed with TeO_2 NPs (10 wt.-%), (c) AP mixed with g-C_3N_4 (10 wt.-%), (d) AP mixed with TeO_2 NPs and g-C_3N_4 (10 wt.-%), and (e) AP mixed with the TeO_2NPs/g-C_3N_4 hybrid composite material (10 wt.-%). (f) Decomposition temperature differences in the HTD of AP and AP with the three additives.

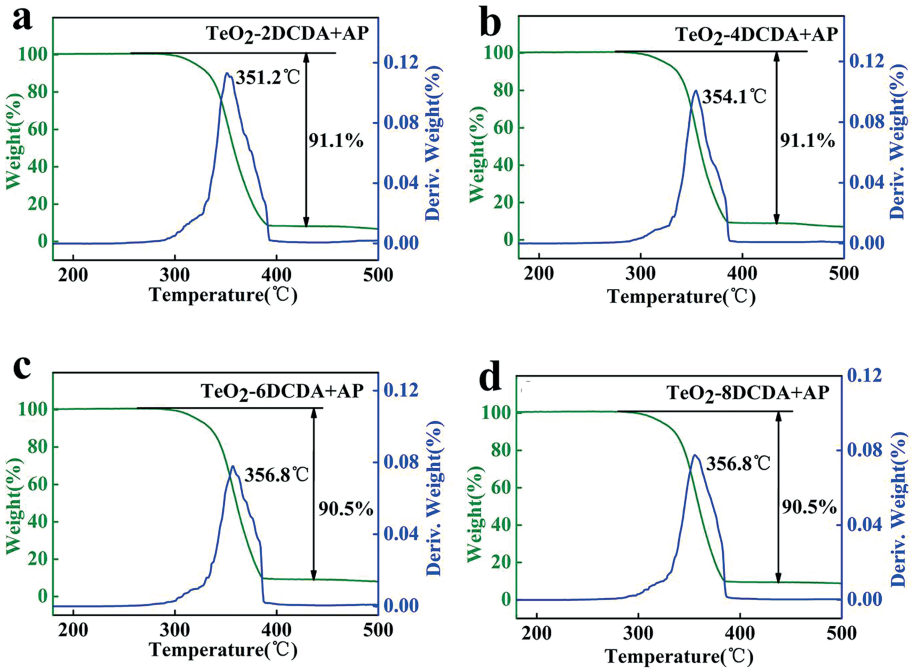

Figure 4. TGA–DTG curves of mixtures of AP with the production of (a) TeO_2–2DCDA, (b) TeO_2–4DCDA, (c) TeO_2–6DCDA, and (d) TeO_2–8DCDA (d).

of AP mixed with the TeO_2NPs/g-C_3N_4 hybrids (Figure 3, e) shows that the HTD temperature is decreased to 350.4 °C. The clear change highlights the promotion effect of the TeO_2 NPs. Moreover, the temperature differences in the HTD of AP mixed with the three additives are shown in Figure 3 (f). All the results confirm that the TeO_2NPs/g-C_3N_4 hybrids are good catalysts for the thermal decomposition of AP.

To better study the catalytic performance of the TeO_2NPs/g-C_3N_4 hybrids with different ratios, the calcined products of TeO_2–*x*DCDA (*x* = 2, 4, 6, 8, and 10 wt.-%) mixed with AP were investigated by TGA–DTG tests for the thermal decomposition of AP. As indicated in Figure 4 (a), the TGA–DTG curve of TeO_2–2DCDA exhibits a single exothermic peak (351.2 °C for HTD). The weight loss ratio reaches up to 91.1 ± 0.5%, which corresponds to the weight of TeO_2–2DCDA (10 ± 0.2 wt.-%). As to TeO_2–4DCDA (Figure 4, b), TeO_2–6DCDA (Figure 4, c), and TeO_2–8DCDA (Figure 4, d), the HTD temperatures of AP are 354.1, 356.8, and 356.8 °C, respectively, with weight loss ratios up to 91.1 ± 0.5, 90.5 ± 0.5, and 90.5 ± 0.5%, respectively. With an increase in the weight of DCDA, the HTD temperature increases and the weight loss ratio decreases slightly because of the sublimation of TeO_2.[14e,21a] The above results indicate that the TeO_2NPs/g-C_3N_4 hybrids are good catalysts for the thermal decomposition of AP.

Catalytic Mechanisms

Jacobs[25] proposed a catalytic mechanism for the thermal decomposition of AP for the first time. The details are as follows:

$$NH_3^+HClO_4^- \rightleftharpoons NH_3\text{-}H\text{-}ClO_4 \rightleftharpoons NH_3\text{-}HClO_4 \rightleftharpoons NH_3(a) + HClO_4(a) \quad (LTD) \quad (1)$$

$$NH_3(a)+HClO_4(a) \rightleftharpoons NH_3(g) + HClO_4(g) \quad (HTD) \quad (2)$$

As is well known, there is a pair of ions (NH_4^+ and ClO_4^-) in the $NH_4^+ClO_4^-$ lattice. The LTD was confirmed to be a heterogeneous process. Namely, proton transfer from NH_4^+ to ClO_4^-, which leads to the formation of NH_3 and $HClO_4$. Subsequently, in the HTD process, gas-phase molecules of NH_3 and $HClO_4$ separate from the AP lattice, which results in the decomposition of AP. Clearly, the exothermic process of the HTD is the result of the oxidation of NH_3 and the reduction of $HClO_4$.[2a,26]

So, how do the TeO_2NPs/g-C_3N_4 hybrids catalyze the thermal decomposition of AP, and what is the role of TeO_2? Obviously, as a semiconductor material, TeO_2 might not only prevent the agglomeration of the catalyst nanoparticles during the preparation, but also offer some synergetic enhancement of the catalytic activity by forming the hybrid structure.[27] TeO_2, which indicated a decrease in the charge-transfer resistance on the g-C_3N_4 surface leading to an effective electron–hole pair separation, as a result showed higher synergetic catalytic effects. Furthermore, the process is very similar to that of the previous paper.[17] We propose a catalytic mechanism involving two steps, including separation of a gas-phase molecule of $HClO_4$ and the oxidation of $HClO_4$. For the first step, as can be seen from Equations (1) and (2), the adsorption of $HClO_4$ and NH_3 on the surface of AP during the LTD process as well as the reduction of $HClO_4$ plays a key role in the thermal decompo-

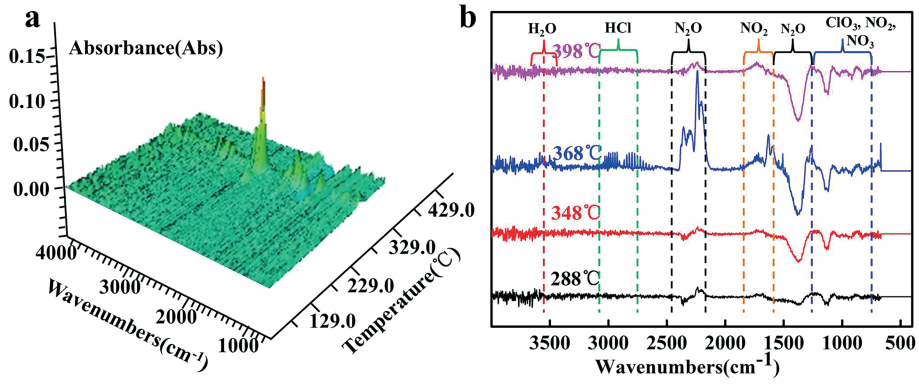

Figure 5. (a) Three-dimensional TGA–FTIR spectra of the gas products in the thermal decomposition of AP. (b) FTIR spectra of gas products formed during decomposition of AP at respective peaks.

sition of AP. In the primary decomposition stage of AP, the adsorption of $HClO_4$ in the pores of AP prevents decomposition of AP because Equation (2) is reversible.[28] On the other hand, g-C_3N_4, as a Lewis base, reacts with $HClO_4$ by Lewis acid–base interaction, which leads to separation of $HClO_4$ from the pores of AP, and the decomposition reaction is pushed toward the right-hand side of Equation (2).

For the second step, g-C_3N_4, as a polymer semiconductor (E_g = 2.7 eV), can easily meet the requirements of heat excitation.[29] Therefore, the conduction-band electrons (e_{cb}^-) and the valence-band holes (h^+) are generated on the surface of g-C_3N_4 under heat excitation.[12c,16a] During the catalytic process, the generated electrons react with $HClO_4$, which results in the reduction of $HClO_4$ to a superoxide radical anion $^{\cdot}O_2^-$. Thermogenerated $^{\cdot}O_2^-$ and h^+ have powerful oxidation ability, and they can further react with NH_3 to form H_2O, NO_2, and N_2O.[12b]

For the purpose to detect the products of the thermal decomposition of AP, TGA–FTIR spectroscopy, as a special analytical instrument, was used to analyze the whole decomposition process by real-time monitoring. Figure 5 (a) shows the three-dimensional TGA–FTIR spectra for the decomposition of AP with 10 wt.-% of the TeO_2NPs/g-C_3N_4 hybrid additives.

Figure 5 (b) shows the FTIR spectra of the gas products formed during decomposition at their respective peaks. All of the evolved products result from the two decomposition stages of the LTD and HTD segment (310–350 and 350–400 °C). The gas products at 368 °C were identified as H_2O/NH_3 ($\tilde{\nu}$ = 3400–3650/1650–1620 cm^{-1}), HCl ($\tilde{\nu}$ = 1750–3000 cm^{-1}),[30] N_2O/NO_2 (2202–2238/1380–1320/840–800 cm^{-1}), and ClO_3 ($\tilde{\nu}$ = 1000–900 cm^{-1}).[14d] In addition, the gas products of decomposition at 398, 368, 348, and 288 °C also confirmed the existence of the above gases. The results of TGA–FTIR spectroscopy show that the main gas products of AP are H_2O, HCl, N_2O, NO_2, and ClO_3.

In brief, the catalytic process is indicated in Figure 6.

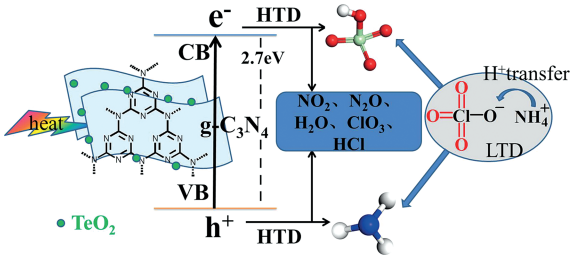

Figure 6. Schematic of the thermal decomposition of AP with the TeO_2NPs/g-C_3N_4 hybrids as additives; CB = conduction band, VB = valence band.

Conclusions

In summary, TeO_2 nanoparticle/graphitic carbon nitride (g-C_3N_4) hybrids were successfully prepared. It was proven that the as-prepared hybrids could be used as excellent catalysts for the thermal decomposition of ammonium perchlorate (AP). The high-temperature thermal decomposition temperature of AP was decreased by 104.4 °C if the TeO_2NPs/g-C_3N_4 hybrid was added to the system. Notably, a catalytic mechanism based on Lewis acid–base interactions was proposed to understand the thermal decomposition of AP. Moreover, the g-C_3N_4-based hybrids as novel catalysts provided insight into the thermal decomposition of AP.

Experimental Section

Materials: Dicyandiamide (DCDA, 99%), high-purity TeO_2 (99.999%, 100–200 nm), and ammonium perchlorate (AR, d_{50}:135 μm) were purchased from Aladdin (Shanghai, China). Tubular furnace atmosphere was obtained from Zhonghuan experiment electric furnace (Tianjin, China). All reagents were of analytic grade and were used without further purification.

Characterization: Powder X-ray diffraction (XRD) patterns were collected from the prepared samples by using a Philips X′Pert Pro X-ray diffractometer by employing Cu-K_α radiation (λ = 0.15418 nm). Field-emission scanning electron microscopy (FESEM, Ultra 55) measurements with an acceleration voltage of 15.0 kV were performed to determine the microstructure of the samples. FTIR spectra were recorded with a Nicolet-5700 FTIR spectrometer by using pressed KBr pellets to test the chemical bonding of the samples from 4000 to 400 cm^{-1}. X-ray photoelectron spectroscopy (XPS) was performed with an ESCALAB 250 electron spectrometer by using Al-K irradiation. The Brunauer–

Emmett–Teller (BET) surface area of the as-prepared sample was determined by physisorption of N_2 at 77 K by using a NOVA 3000 surface area.

Experimental Methods: The TeO_2NPs/g-C_3N_4 hybrids were prepared by a general method that involved placing a ground mixture of highly pure TeO_2 particles and DCDA (molar ratio equal 1:1) in a tubular furnace atmosphere followed by calcination at 550 °C under argon flow with a heating rate of 2.5 K min^{-1}.

Catalytic Measurements: To test the catalytic effect of the TeO_2NPs/g-C_3N_4 hybrids on the thermal decomposition of AP, AP and the TeO_2NPs/g-C_3N_4 hybrids with different weight ratios were mixed and ground for 1 h. The resulting mixture was detected by thermogravimetric analysis/differential scanning calorimetry (TGA-DSC) by using a Mettler Toledo TGA-DSC1–1100LF and differential thermal analyzer (DTA QD-600) at a heating rate of 10 °C min^{-1} under a static N_2 atmosphere over the temperature range of 25 to 500 °C. Thermogravimetric analysis–Fourier transform infrared (TGA–FTIR), as a special technic, was used to analyze the catalytic mechanism of the thermal decomposition of AP by detecting the products formed during the decomposition process in real time.

Acknowledgments

The authors are grateful for financial support from the National Natural Science Foundation of China (NSFC) (project numbers 51372211, 10576026, and 21301142), National Defense Fundamental Research Projects (project number A3120133002), Youth Innovation Research Team of Sichuan for Carbon Nanomaterials (grant number 2011JTD0017), Applied Basic Research Program of Sichuan Province (grant number 2014JY0170), and Postgraduate Innovation Fund Project by Southwest University of Science and Technology (grant number 15ycx007).

[1] a) P. W. M. C. Jacobs, H. M. Whitehead, *Chem. Rev.* **1969**, *69*, 551–590; b) I. P. S. Kapoor, P. Srivastava, G. Singh, *Propellants Explos. Pyrotech.* **2009**, *4*, 351–356; c) K. Kishore, G. Prasad, *Def. Sci. J.* **2014**, *29*, 39–54.
[2] a) V. Boldyrev, *Thermochim. Acta* **2006**, *443*, 1–36; b) S. Vyazovkin, C. A. Wight, *Chem. Mater.* **1999**, *11*, 3386–3393.
[3] L. Chen, G. Li, L. Li, *J. Therm. Anal. Calorim.* **2008**, *2*, 581–587.
[4] a) L. Li, X. Sun, X. Qiu, J. Xu, G. Li, *Inorg. Chem.* **2008**, *47*, 8839–8846; b) M. Zhou, X. Jiang, L. Lu, X. Wang, *J. Hazard. Mater.* **2012**, *225–226*, 124–130.
[5] S. Lu, X. Jing, J. Liu, J. Wang, Q. Liu, Y. Zhao, *J. Solid State Chem.* **2013**, *197*, 345–351.
[6] G. Tang, S. Tian, Z. Zhou, Y. Wen, A. Pang, Y. Zhang, D. Zeng, H. Li, B. Shan, C. Xie, *J. Phys. Chem. C* **2014**, *118*, 11833–11841.
[7] W. Zhang, Q. Luo, X. Duan, Y. Zhou, C. Pei, *Mater. Res. Bull.* **2014**, *50*, 73–78.
[8] R. A. Chandru, S. Patra, C. Oommen, N. Munichandraiah, B. N. Raghunandan, *J. Mater. Chem.* **2012**, *22*, 6536–6538.
[9] N. Li, Z. Geng, M. Cao, L. Ren, X. Zhao, B. Liu, *Carbon* **2013**, *54*, 124–132.
[10] X. Guan, L. Li, J. Zheng, G. Li, *RSC Adv.* **2011**, *1*, 1808–1814.
[11] Y. Wang, J. Zhu, X. Yang, L. Lu, X. Wang, *Thermochim. Acta* **2005**, *437*, 106–109.
[12] a) T. Sekine, H. Kanda, Y. Bando, M. Yokoyama, *J. Mater. Sci. Lett.* **1990**, *9*, 1376–1378; b) X. Wang, S. Blechert, M. Antonietti, *ACS Catal.* **2012**, *2*, 1596–1606; c) X. Wang, X. Chen, A. Thomas, X. Fu, M. Antonietti, *Adv. Mater.* **2009**, *21*, 1609–1612; d) Y. Wang, J. Zhang, X. Wang, M. Antonietti, H. Li, *Angew. Chem. Int. Ed.* **2010**, *49*, 3356–3359; *Angew. Chem.* **2010**, *122*, 3428–3431.
[13] a) X. Wang, K. Maeda, A. Thomas, K. Takanabe, G. Xin, J. M. Carlsson, *Nat. Mater.* **2009**, *8*, 76–80; b) A. Thomas, A. Fischer, F. Goettmann, M. Antonietti, J. O. Müller, R. Schlögl, J. M. Carlsson, *J. Mater. Chem.* **2008**, *18*, 4893–4908.
[14] a) B. Jürgens, E. Irran, J. Senker, P. Kroll, H. Müller, W. Schnick, *J. Am. Chem. Soc.* **2003**, *125*, 10288–10300; b) C. P. Grey, N. J. Dupré, *Chem. Rev.* **2004**, *104*, 4493–4512; c) G. Algara-Siller, N. Severin, S. Y. Chong, T. Björkman, R. G. Palgrave, A. Laybourn, M. Antonietti, Y. Z. Khimyak, A. V. Krasheninnikov, J. P. Rabe, U. Kaiser, A. I. Cooper, A. Thomas, M. J. Bojdys, *Angew. Chem. Int. Ed.* **2014**, *53*, 7450–7455; *Angew. Chem.* **2014**, *126*, 7580–7585; d) Q. Li, Y. He, R. Peng, *RSC Adv.* **2015**, *5*, 24507–24512; e) T. Ma, Y. Tang, S. Dai, S. J. Qiao, *Phys. Small* **2014**, *12*, 2382–2389.
[15] M. Shalom, S. Inal, D. Neherb, M. Antonietti, *Catal. Today* **2014**, *225*, 185–190.
[16] a) L. Zhang, D. Jing, X. She, H. Liu, D. Yang, Y. Lu, *J. Mater. Chem. A* **2014**, *2*, 2071–2078; b) D. J. Martin, K. Qiu, S. A. Shevlin, A. D. Handoko, X. Chen, Z. Guo, J. Tang, *Angew. Chem. Int. Ed.* **2014**, *53*, 9240–9245; *Angew. Chem.* **2014**, *126*, 9394–9399.
[17] S. Zhang, J. Li, M. Zeng, G. Zhao, J. Xu, W. Hu, X. Wang, *ACS Appl. Mater. Interfaces* **2013**, *5*, 12735–12743.
[18] S. Ye, L. Qiu, Y. Yuan, Y. Zhu, J. Xia, J. Zhu, *J. Mater. Chem. A* **2013**, *1*, 3008–3015.
[19] I. P. Kondratyuk, L. A. Muradyan, Y. V. Pisarevskii, V. I, J. Simonov, *Kristallografiya* **1987**, *32*, 354–359.
[20] a) T. Komatsu, H. Tawarayama, H. Mohri, K. Matusita, *J. Non-Cryst. Solids* **1991**, *2*, 105–113; b) M. A. Hassan, C. A. Hogarth, *J. Mater. Sci.* **1988**, *23*, 2500–2504; c) M. Ceriotti, F. Pietrucci, M. J. Bernasconi, *Phys. Rev. B* **2006**, *10*, 1–20.
[21] a) O. Noguera, T. Merle-Méjean, A. P. Mirgorodsky, M. B. Smirnov, P. Thomas, J.-C. Champarnaud-Mesjard, *J. Non-Cryst. Solids* **2003**, *1*, 50–60; b) S.-H. Kim, Y. Yoko, S. Sakka, *J. Am. Ceram. Soc.* **1993**, *76*, 2486–2490.
[22] X. Lu, K. Xu, P. Chen, K. Jia, S. Liu, C. Wu, *J. Mater. Chem. A* **2014**, *2*, 18924–18928.
[23] a) A. Vinu, K. Ariga, T. Mori, T. Nakanishi, S. Hishita, D. Golberg, Y. Bando, *Adv. Mater.* **2005**, *17*, 1648–1652; b) Y. Wang, X. Wang, M. Antonietti, Y. Zhang, *ChemSusChem* **2010**, *3*, 435–439; c) B. V. R. Chowdari, P. P. Kumari, *J. Non-Cryst. Solids* **1996**, *1*, 31–40; d) T. Sun, S. P. Buchner, N. E. Byer, *J. Vac. Sci. Technol.* **1980**, *5*, 1067–1073; e) M. K. Bahl, K. L. Watson, K. J. Irgolic, *J. Chem. Phys.* **1977**, *66*, 5526–5535; f) L. Fan, Y. Hu, J. Maier, P. Adelhelm, B. Smarsly, M. Antoniettii, *Adv. Funct. Mater.* **2007**, *17*, 3083–3087.
[24] D. L. Reid, A. E. Russo, R. V. Carro, M. A. Stephens, A. R. LePage, T. C. Spalding, *Nano Lett.* **2007**, *7*, 2157–2161.
[25] P. W. M. Jacobs, A. Russell-Jones, *J. Phys. Chem.* **1968**, *72*, 202–207.
[26] E. F. Khairetdinov, V. V. Boldyrev, *Thermochim. Acta* **1980**, *41*, 63–68.
[27] a) Y. Zhang, M. Antonietti, *Chem. Asian J.* **2010**, *5*, 1307–1311; b) M. F. Al-Kuhaili, S. M. A. Durrani, E. E. Khawaja, J. Shirokoff, *J. Phys. D: Appl. Phys.* **2002**, *35*, 910–915; c) S. K. J. Al-Ani, C. A. Hogarth, *Int. J. Electron.* **1985**, *58*, 123–131; d) M. Abhai, K. Shiv, *Thin Solid Films* **1988**, *161*, 101–106.
[28] G. Shen, D. Chen, C. J. Lee, *J. Phys. Chem. B* **2006**, *110*, 15689–15693.
[29] A. M. Stoneham, *Rep. Prog. Phys.* **1981**, *44*, 1251–1295.
[30] http://webbook.nist.gov/chemistry/form-ser.html.

Received: May 10, 2015
Published Online: August 6, 2015

